A STUDY OF GRID RESOLUTION, TRANSITION AND TURBULENCE MODEL USING THE TRANSONIC SIMPLE STRAKED DELTA WING

Robert E. Bartels

Aeroelasticity Branch, NASA Langley Research Center
M.S. 340, Hampton, VA 23681-0001
e-mail: r.e.bartels@larc.nasa.gov

Key words: Straked delta wing, vortex, turbulence modeling, turbulent transition

Abstract. Three-dimensional transonic flow over a delta wing is investigated using several turbulence models. The performance of linear eddy viscosity models and an explicit algebraic stress model is assessed at the start of vortex flow, and the results compared with experimental data. To assess the effect of transition location, computations that either fix transition aft of the leading edge or are fully turbulent are performed. These computations show that grid resolution, transition location and turbulence model significantly affect the 3D flowfield.

1 INTRODUCTION

Recent flight phenomena of interest to aerodynamicists have highlighted the need for better understanding of flowfields about high performance aircraft configurations. Among various factors to which complex flow fields are sensitive, turbulence and transition can in some cases significantly impact static and unsteady wing loading. Turbulence models suitable for practical applications have been proposed ranging in complexity from the zero, one- and two-equation eddy viscosity models to full Reynolds stress closures. Among those, one- and two-equation models such as the k-ε or the k-ω shear stress transport (SST) models, solve transport equations for important physical parameters. Other transport models such as the Spalart-Allmaras (SA) are widely used although based more on empiricism. None of these models simulate anisotropies in turbulent stresses. Anisotropic eddy-viscosity models have been developed to overcome this deficiency. Explicit algebraic stress models (EASMs), based on the initial work of Pope[1] and later generalized by Gatski and Speziale[2], are related to anisotropic eddy viscosity models, but depend on both rotational and irrotational strain rates.

Computational investigations of delta wings have typically focused on geometric or flow modeling issues, or have attempted to simulate vortex development, instability or breakdown. Recent efforts have made use of the Euler equations[3-5] , laminar[5-6] and turbulent Navier-Stokes equations with zero- and one-equation turbulence models.[5,7-9] One study found that the primary vortex location and vorticity level over a delta wing are altered very little by viscous effects, although viscous solutions exhibited secondary and tertiary vortices not seen in the Euler solutions.[5] Another work points out that important flow details are obtained only by a viscous solution.[4] For example, significant flow separation over the wing can alter the vortex location. Turbulent transonic flow computations for another delta wing revealed little difference between the Baldwin-Lomax and the Johnson-King turbulence models.[8] In another study of a similar delta wing, the Degani-Schiff and the Johnson-King models showed similar results, while results with the Baldwin-Lomax model differed somewhat from the results of the other two models.[4] It is clear that the non-equilibrium effects embodied in the Johnson-King model were not important in those cases. Yet one would expect that the isotropic eddy viscosity turbulence models used in the previous examples are not completely adequate for complex three-dimensional vortex delta wing flows. Whether or not the anisotropic eddy

viscosity of an explicit algebraic eddy viscosity model will offer an improvement remains an open question. It may be that grid resolution and other grid related issues are as significant or more so than turbulence modeling.[4]

Recent experimental studies using a simple straked delta wing have been performed at low to transonic speeds.[10-13] These studies have produced a large body of pressure data, light sheet visualization and some particle image velocimetry data for fixed and oscillating incidence wings at several Mach numbers over a range of incidences. Published test results offer quite complex three-dimensional low speed and transonic flowfields. Although no detailed turbulence data has yet been published, pressure and visualization data from the tests reveal interesting phenomena such as self-induced shock/vortex oscillation and finger shocklets at certain incidences at very high subsonic speeds.

The sectional and planform shapes of the low speed and transonic models were somewhat different. One key difference is a transition strip near the leading edge of the outboard panel of the transonic wing. A partial span transition strip necessitates the use of turbulence modeling in the simulation of the transonic flow, but also allows an analysis of the turbulence model and transition location as separate effects. Several computational studies have made use of the low speed data,[14-16] however, none have focused on the effect of the turbulence model and transition on the simulation of the transonic vortex flow. The effect of turbulence model and transition location on the straked delta wing at fixed incidence has been investigated recently for several conditions near the start of vortex flow.[17] Key results from that study are summarized in the present paper.

2 METHOD

The computer code CFL3D is used in the present study. That code solves the three-dimensional thin-layer Reynolds averaged Navier-Stokes equations using an upwind finite volume formulation.[18] It is capable of solving multiple zone grids with one-to-one connectivity. Grid sequencing and local time stepping for convergence acceleration to a steady state are employed. Upwind-biased spatial differencing is used for the inviscid terms with flux limiting in the presence of shocks. The viscous terms are centrally differenced. Cross diffusion terms are neglected in the thin-layer formulation of the equations. The flux-difference splitting method of Roe[19] is employed to obtain fluxes at cell faces. The turbulence models are solved uncoupled from the flow equations. Details of the SA and the SST turbulence models can be found in their respective references.[20, 21] The form of the Gatski-Speziale EASM model used includes turbulence anisotropy effects. Additional details of the Gatski-Speziale k-ε EASM model and its implementation in CFL3D are discussed in Reference 22.

3 TRANSONIC SIMPLE STRAKE DELTA WING MODEL AND GRID

Figures 1-2 present the transonic simple strake delta wing planform layout. Figure 1 shows the planform of the strake and outboard wing panel. A transition strip is shown extending over the span of the outboard panel. The outboard panel of the physical model had a transition strip a distance 14.5 mm aft of the leading edge, measured perpendicular to the leading edge. Note that Reference 17 misprints this as 14.5% rather than 14.5 mm. Computational modeling of the transition strip will be discussed in a later section. Figure 2 shows the layout of the pressure sections. There are four chordwise pressure sections on the outboard wing and three spanwise pressure sections spanning the strake to outer wing panel.[10-13, 17] The coordinate

system also shown in that figure has the strake leading edge as origin. Pressure section locations presented in the figures to follow are based on this coordinate system.

The optimal grid for a delta wing is a conical grid.[23] Some geometries can present difficulties; in the present case, it is the need to model the partial span transition strip behind the leading edge of the outer delta wing panel. To accommodate a partial span transition strip, a C-H grid is used here that is divided into multiple blocks. The combined surface grids for this wing are shown in Figure 3. An inboard block covers the strake and all surface grid points down stream of the strake. The outboard block covers all the wing surface grids outboard of the strake delta junction. Using this multiblock strategy, it is possible to turn on the turbulence production terms over the entire outboard delta wing panel aft of the grid line at the transition strip location, while otherwise including the convective and diffusive terms of the one- and two-equation turbulence models throughout the flowfield.

In the present computations a moderately refined mesh has been used in most cases, from here on called the standard grid. This mesh is used because of the potentially large added computational effort required for the turbulence models that will be used and to allow unsteady computations to be performed in a reasonable amount of time. The multi-block standard grid is composed of 4 blocks, which if combined into a single mesh would comprise a C-H mesh with 153×65×57 grids in the streamwise, spanwise and normal directions. The isometric drawing of Figure 3 shows the wing, symmetry and wake plane surface grids. Spacing of the viscous grid at the wing surface in the normal direction is 1×10^{-7} and 1×10^{-6} (nondimensionalized by chord) at the leading and trailing edges, respectively. The grid approximates a semi-infinite flowfield with an inviscid symmetry plane at the wing root. It extends 5.5 chord lengths up and downstream from the wing and 5.5 chord lengths away from the wing tip.

4 RESULTS

The cases analyzed in References 10-13 cover angles of attack from zero to beyond vortex bursting, at Mach numbers of 0.225, 0.60 and 0.90. Cunningham and Geurts found a dramatic shift in the character of the flow between the Mach numbers of 0.60 and 0.90.[13] At the higher Mach number a shock significantly alters the flowfield, inducing leading edge and shock-induced trailing edge separations. These features appear at an angle of attack at which vortex flow begins. Conditions at the start of vortex flow will be considered in the present report. As summarized in Table 1, the experimental data and computed solutions are at freestream Mach numbers of 0.60 and 0.90 and a Reynolds number of 8 million. The test conditions being considered are NLR SIS run number 330 (Cases 1-6) at Mach number 0.60 and numbers 504 (Case 7) and 506 (Case 8-11) at a Mach number of 0.90. Other key factors are found to influence the present computational results. They are the grid, turbulent transition location and turbulence model. The following sections discuss these aspects and their influence on the solutions at the two Mach numbers.

4.1 Effect of grid resolution

In an attempt to assess the adequacy of the grid, a resolution study is conducted using fine, medium and coarse grids. These grids are constructed from a fine grid that has combined dimensions of 233×105×89 grid points in the streamwise, spanwise and normal directions. This mesh is divided into six blocks. Medium and coarse grids are constructed by eliminating

every other grid point from each of the six blocks in the fine and medium grids. The standard grid, discussed earlier, has a resolution that is between that of the medium and fine grids.

Results from this study are found in Table 1 and in Figures 4 and 5. The coarse, medium and fine grid solutions correspond to cases 1-3 in Table 1. The moment coefficient is shown converging to the experimental value, but it is clear that the force coefficient is not entirely convergent even at the finest grid level. The area of the wing responsible for the incomplete convergence of the force coefficient can be found by examining pressure distributions in sections 1, 2 and 6 in Figures 4 and 5. These pressures reveal an inadequate resolution of the suction peaks of the strake and wing vortices. Away from the early development of the vortices at the leading edge and strake, the fine grid does appear to sufficiently resolve the flowfield.

Resolution of the vortex core and capture of the suction peak are recognized as important, in some cases critical, to a globally correct modeling vortex dominated flows. Yet in spite of the incomplete grid resolution in the vortex core regions, the standard grid will be used in all of the remaining computations. The use of this grid is forced by the limitation imposed by computing several unsteady solutions. It may be possible in the future to perform parallel computations for the same problem and turbulence models using a much finer grid. Therefore, the present study must be seen as a preliminary assessment of advanced turbulence models for these flows. As seen by comparing cases 1-3 and 4 in Table 1, force and moment coefficients using the standard grid lie between those of the medium and fine grids. It is also reassuring that pressure distributions in Figures 4 and 5 using the standard grid fall roughly between those of the medium and fine grids. Different transition locations also contribute somewhat to the difference in results of case 4 compared to those of cases 1-3. This effect will be addressed in a larger context in the next section.

The grid resolution study of cases 1-3 is performed at a Mach number of 0.60. At this Mach number the force and moment coefficients computed with the medium and fine grids differ from experiment by less than 4%. Computations at a Mach number of 0.90 (cases 7-11 in Table 1, and Figures 6 and 7) with the standard grid paint a much different picture. At this Mach number computed force coefficients differ from experiment by up to 7% (case 7) and moment coefficients differ from 50% (case 11) to 80% (cases 8-10). It is possible that the high subsonic flow requires additional resolution in at least some areas that differ from those requiring resolution at the lower Mach number. The lower Mach number upper surface flow is largely subsonic with very high pressure gradients only near vortices. At the higher Mach number, most of the wing upper surface flow is supersonic with much flatter pressure gradients over most of the wing, including the wing and strake vortices. The later flowfield also involves incipient shock separation. If the high subsonic flow requires significantly more grid resolution or a redistribution of grids, the limitations addressed earlier regarding grid convergence and the use of a single grid for all computations are only accentuated. This issue will not be fully addressed in this paper. It will be assumed in the remainder of the computations that the effect of transition location and turbulence model can be addressed at least initially with the standard grid, recognizing that some of the cases examined will require further study.

4.2 Effect of transition

In addition to the influence of grid, the force and moment coefficient data of cases 8 and 11 point to another important influence, namely that of transition location. To facilitate a study

of this effect, several different locations have been simulated. Computations designated as fully turbulent (transition location at 'le' in Table 1) include turbulence production terms starting from the leading edge. Computations designated with other transition locations model a transition strip. The outer panel transition strip is modeled computationally by turning on turbulence production terms at a grid line that is located at 5-6% from the leading edge based on local wing chord. This location very roughly corresponds to 14.5 mm aft of the leading edge on the physical wing model. Over the strake, turbulence production terms are turned on at approximately the 95% chord location. This transition location has been chosen for several reasons. Unpublished pressure contours computed by the author at a Mach number of 0.899 and angle of attack of 11.39^{o} show a long region of accelerating supersonic flow over the strake. Continuous flow acceleration can be observed in the inboard pressure distributions at sections 5-7 in Figure 7. Deceleration over the strake starts at around 70-80% chord. It is not unreasonable to assume that laminar or relaminarized flow persists over most or all of the accelerating flow. The second reason is that a transition location for the inboard panel at 95% resulted in the best match with the pressure data in the area of the strake. Computations were performed at a Mach number of 0.899 and angle of attack of 11.39^{o} with transition on the strake at the leading edge, 70% and 95% chord with the later matching best with experiment. The discussion to follow sheds additional light on the effect of transition location.

Case 8 is computed with the SA turbulence model with transition set at the leading edge, i.e. fully turbulent. That solution was computed in steady state mode to a converged steady state. The force and moment coefficients in Table 1 and the pressures in Figures 6 and 7 are steady. Case 11 is computed using the SA model with transition at the 95% (strake) and 6% (outer wing panel) local chord locations. Steady computations of case 11 did not reach a converged steady state, but instead reached what appeared to be a limit cycle. To confirm a true limit cycle, time accurate computations were continued until a constant amplitude limit cycle solution was indeed obtained. Sustained limit cycle oscillations for over at least 50 cycles were computed. Accordingly, the force and moment coefficient data for case 11 in Table 1 and the pressure distributions in Figures 8 and 9 for case 11 are mean values. Setting aside for the present the unsteady nature of the solution in case 11, attention is directed to force and moment data for cases 8 and 11. Observation of this data in Table 1 leads one to conclude that modeling transition significantly improves the comparison with experiment. The reason for that improvement can be found by comparing the SA model pressures in Figures 6 and 7 with those of Figures 8 and 9. The pressure distribution of section 7 in Figure 7 compared with that in Figure 9 shows that most of the improvement seen in Figure 9 is localized to the trailing edge region of the strake. The forward strake sections 5 and 6 are improved only slightly. By comparing Figures 6 and 8, a moderate improvement can be seen in the pressures of sections 1-4. To conclude, at the high subsonic Mach number, transition plays a greater role in accurate computation of wing loading than it does at a lower subsonic Mach number. At the high subsonic Mach number pressures over the entire wing correlate better with experiment, with the greatest improvement in the inboard regions of the aft spanwise section 7.

The experimental data show a change in character from quasi steady at 9.38 degrees to unsteady limit cycle oscillation of the shock and vortices at an angle of attack of 11.39 degrees.[13] This change from steady flow at 9 degrees to unsteady flow at 11 degrees also appears to be captured in the present computations. Case 7 in Table 1 presents data at Mach number 0.90 and angle of attack at 9.38^{o}, computed with transition locations set at the 95% (strake) and 6% (outer wing panel) chord locations. The unsteady computation of this case yielded a damped oscillatory solution that reached a steady state, i.e. zero oscillatory amplitude. The solution with identical transition and turbulence modeling, at 11.94 degrees

and a Mach number of 0.60 also reached a steady state. All of the fully turbulent solutions at 11.39 degrees, shown in Figures 6 and 7, also reached a steady state while the solution of case 11 reached a steady state limit cycle oscillation.

4.3 Effect of turbulence model

Computed results using the explicit algebraic stress model of Gatski and Speziale [2, 22] (EASM), the Spalart-Allmaras model (SA) [20], the k-ω shear stress transport model (SST) [21] are shown in cases 4-6 and 8-10 in Table 1 and Figures 6 and 7. Cases 4-6 are at a Mach number 0.601 and have transition location set at 95% (strake) and 6% (outer wing panel). All three turbulence models perform well at this condition with deviations in force and moment coefficient ranging from 3-7%. At this Mach number the EASM does not appear to offer any advantage. Cases 8-10 at a Mach number 0.899 have transition set at the leading edge. It has already been established that at this Mach number transition location plays a significant role. Turbulence model also emerges as a strong influence. A comparison of force and moment coefficients computed by the three models with experiment show that a significant improvement is achieved by use of the EASM model. Figures 6 and 7 show that improvement to be found mainly in the outboard sections of the wing. (sections 1-4, and section 7) Figures 8 and 9 compare pressure distributions derived using the SA model in case 11 with those computed using the EASM turbulence model in case 10. It is clear from Figures 8 and 9 that transition modeling improves pressures in the aft portion of the strake while the nonlinear eddy viscosity of the EASM model improves pressures on the outboard sections of the wing.

5 CONCLUDING REMARKS

A computational study of the effect of grid resolution, turbulent transition location and turbulence model has been performed at transonic Mach numbers of 0.60 and 0.90 using the transonic simple straked delta wing. This study has shown that all three effects play important but different roles.

Grid resolution has been studied at the lower Mach number and found to be important. The early development of the strake and wing vortices is not fully resolved even with the finest grid. Down stream vortex development with the finest grid, and in areas away from the vortex, however, appeared to match experiment very well at the lower Mach number. It is expected that it will be important at a high subsonic Mach number since, proper development of the strake and wing vortices requires adequate grid resolution at any Mach number. In addition, resolution of the shock and shock-induced separation are important at the higher Mach number.

The simulation of transition location has a very strong effect on the pressure distribution for the straked delta wing at a high subsonic Mach number at the start of vortex flow. Moment coefficient and the pressures over the aft strake region are better captured with the SA model having a transition location modeled at 95% (strake) and 6% (outboard panel). At the high subsonic Mach number, the computed flowfield simulation that included transition strip location and laminar strake flow has resulted in a limit cycle flow oscillation, whereas the fully turbulent computations with all the turbulence models reached a steady state solution.

With respect to force coefficients, all turbulence models match well at the lower Mach number, while at the high subsonic Mach number, all are significantly off in moment. Nevertheless, the fully turbulent EASM results do yield significant improvement in moment

coefficient at the higher Mach number. The reason for the improvement due to the EASM model is the better match of pressures in the wing tip region. Improvement would be expected if the outboard leading edge and inboard shock separations include significant Reynolds stress anisotropies. Further investigations with better grid resolution are needed to more accurately reproduce results for some of the cases studied.

6 ACKNOWLEDGEMENT

The author thanks Mr. L. J. Hutsell at AFRL/VASV for providing the surface grid file for the transonic simple strake delta wing and Dr. A. M. Cunningham at LMTAS for providing the experimental pressure data.

7 REFERENCES

[1] Pope, S. B., "A more general effective-viscosity hypothesis," *Journal of Fluid Mechanics*, Vol. 72, part 2, 1975, pp. 331-340.

[2] Gatski, T. B. and Speziale, C. G., "On explicit algebraic stress models for complex turbulent flows," *Journal of Fluid Mechanics*, vol. 254, 1993, pp. 59-78.

[3] Hoeijmakers, H. W. M., Jacobs, J. M. J. W., van den Berg, J. I., "*Numerical Simulation of Vortical Flow over a Delta Wing at Subsonic and Transonic Speeds*," NLR TP-90029, September 1990.

[4] Longo, J. M. A., "*Simulation of Complex Inviscid and Viscous Vortex Flow*," Fluid Dynamics of High Angle Attack, IUTAM Symposium Tokyo, Japan, September 13-17, 1992, Kawamura, R., Aihara, Y., eds..

[5] Agrawal, S., Barnett, R. M., Robinson, B. A., "Numerical Investigation of Vortex Breakdown on a Delta Wing," *AIAA Journal*, Vol. 30, No. 3, March 1992, pp. 584-591.

[6] Gordnier, R. E., "Numerical Simulation of a 65-Degree Delta-Wing Flowfield," *Journal of Aircraft*, Vol. 34, No. 4, July-August 1997, pp. 492-499.

[7] Tuncer, I. H. and Platzer, M. F., "Computational Study of Subsonic Flow over a Delta Canard-Wing-Body Configuration," *Journal of Aircraft*, Vol. 35, No. 4, July-August 1998, pp. 554- 560.

[8] Kaynak, U., Tu, E., Dindar, M. and Barlas, R., "*Nonequilibrium Turbulence Modeling Effects on Transonic Vortical Flows about Delta Wings*," AGARD CP-494, Vortex Flow Aerodynamics, July 1, 1991.

[9] Ekaterinaris, J. A. and Schiff, L. B., "*Vortical Flows over Delta Wings and Numerical Prediction of Vortex Breakdown*," AIAA-90-0102, 28th Aerospace Sciences Meeting, January 8-11, 1990, Reno, NV.

[10] Cunningham, A. M., den Boer, R. G., Dogger, C. S. G., Geurts, E. G. M., Retel, *A.* P. and Zwaan, R. J., "*Unsteady Transonic Wind Tunnel Test on a Semi Span Straked Delta Wing Model Oscillating in Pitch, Part 1: Description of Model, Test Setup, Data Acquisition and Data Processing,"* Wright Laboratory report WL-TR-94-3094, December 1994.

[11] Cunningham, A. M. and Geurts, E. G. M., "*Analysis of Limit Cycle Oscillation /Transonic High Alpha Flow Visualization, Part 2: Stationary Model Data,"* Air Force Research Laboratory report AFRL-VA-WP-TR-1998-3004, January 1998.

[12] Cunningham, A. M. and den Boer, R. G., "Low-Speed Unsteady Aerodynamics of a Pitching Strake Wing at High Incidence-Part II: Harmonic Analysis," *Journal of Aircraft*, Vol. 27, No. 1, January 1990, pp. 31-41.

[13] Cunningham, A. M., Geurts, E. G. M., "*Analysis of Limit Cycle*

Oscillation/Transonic High Alpha Flow Visualization, Part 1: Discussion," Air Force Research Laboratory Report AFRL-VA-WP-TR-1998-3003, January 1998.

[14]Kern, S. B., "*Numerical Investigation of Vortex Flow Control Through Small Geometry Modifications at the Strake/Wing Junction of a Cropped Double Delta Wing,*" AIAA-92-0411, 30th Aerospace Sciences Meeting and Exhibit, January 6-9, 1992, Reno, NV.

[15]Ekaterinaris, J. A., Coutley, R. L., Schiff, L. B., Platzer, M. F., "*Numerical Investigation of the Flow over a Double Delta Wing at High Incidence*," AIAA-91-0753, 29th Aerospace Sciences Meeting, January 7-10, 1991, Reno NV.

[16]Ekaterinaris, J. A. and Schiff, L. B., "*Navier-Stokes Solutions for an Oscillating Double-Delta Wing*," AIAA-91-1624, AIAA 22nd Fluid Dynamics, Plasma Dynamics and Lasers Conference, June 24-26, 1991, Honolulu, Hawaii.

[17]Bartels, R. E., Gatski, T. B., "*Prediction of Transonic Vortex Flows Using Linear and Nonlinear Turbulent Eddy Viscosity Models*," NASA TM-2000-210282, May 2000.

[18] Krist, S. L., Biedron, R. T., and Rumsey C. L., "*CFL3D User's Manual (Version 5.0)*," NASA TM-1998-208444, June 1998.

[19] Roe, P. L., "Approximate Riemann Solvers, Parameter Vectors, and Difference Schemes," *Journal of Computational Physics*, Vol. 43, 1981, pp. 357-372.

[20]Spalart, P. R., and Allmaras, S. R., "A One-Equation Turbulence Model for Aerodynamic Flows," *La Recherche Aerospatiale*, No. 1, 1994, pp. 5-21.

[21]Menter, F. R., "Improved Two-Equation *k*-ω Turbulence Models for Aerodynamic Flows," NASA TM 103975, Oct. 1992.

[22]Rumsey,C. L., Gatski, T. B., and Morrison, J. H., "*Turbulence Model Prediction of Extra-Strain Rate Effects in Strongly-Curved Flows*," AIAA paper 99-0157, 37th Aerospace Sciences Meeting and Exhibit, January 11-14, 1999, Reno, NV.

[23]Kumar, A., "Role of flow-consistent grid in CFD," *Computers and Fluids*, Vol. 28, 1999, pp. 265-280.

Case No.	M_∞	α (Deg.)	C_N (Calc.)	C_N (Exp.)	C_m (Calc.)	C_m (Exp.)	Turb. Model	Approx. Strake Transit. Location	Approx. Outbrd Transit. Location	Grid
1	0.601	11.94	0.680	0.65	0.023	0.030	SA	6%	6%	crs
2	0.601	11.94	0.663	0.65	0.028	0.030	SA	6%	6%	med
3	0.601	11.94	0.647	0.65	0.029	0.030	SA	6%	6%	fine
4	0.601	11.94	0.650	0.65	0.028	0.030	SA	95%	6%	stndrd
5	0.601	11.94	0.656	0.65	0.030	0.030	SST	95%	6%	stndrd
6	0.601	11.94	0.640	0.65	0.028	0.030	EASM	95%	6%	stndrd
7	0.900	9.38	0.594	0.64	0.0016	0.005	SA	95%	6%	stndrd
8	0.899	11.39	0.720	0.69	0.0023	0.013	SA	le	le	stndrd
9	0.899	11.39	0.709	0.69	0.0038	0.013	SST	le	le	stndrd
10	0.899	11.39	0.697	0.69	0.0053	0.013	EASM	le	le	stndrd
11	0.899	11.39	0.690‡	0.69	0.0059‡	0.013	SA	95%	6%	stndrd

‡ Mean value

Table 1. Case data

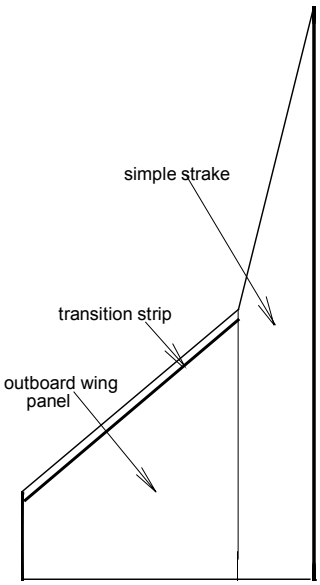

Figure 1. Transonic simple straked delta wing model.

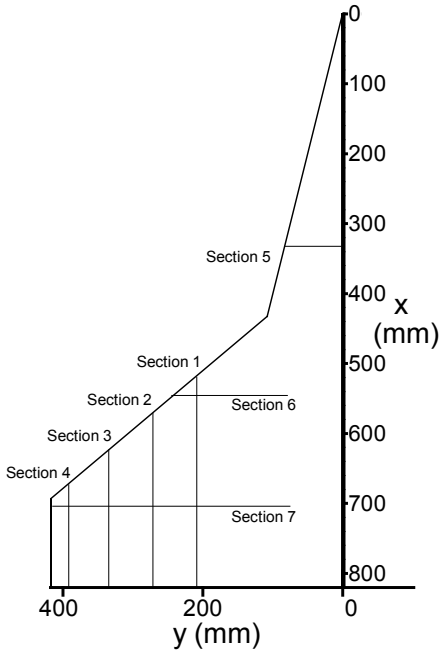

Figure 2. Planform and pressure section layout.

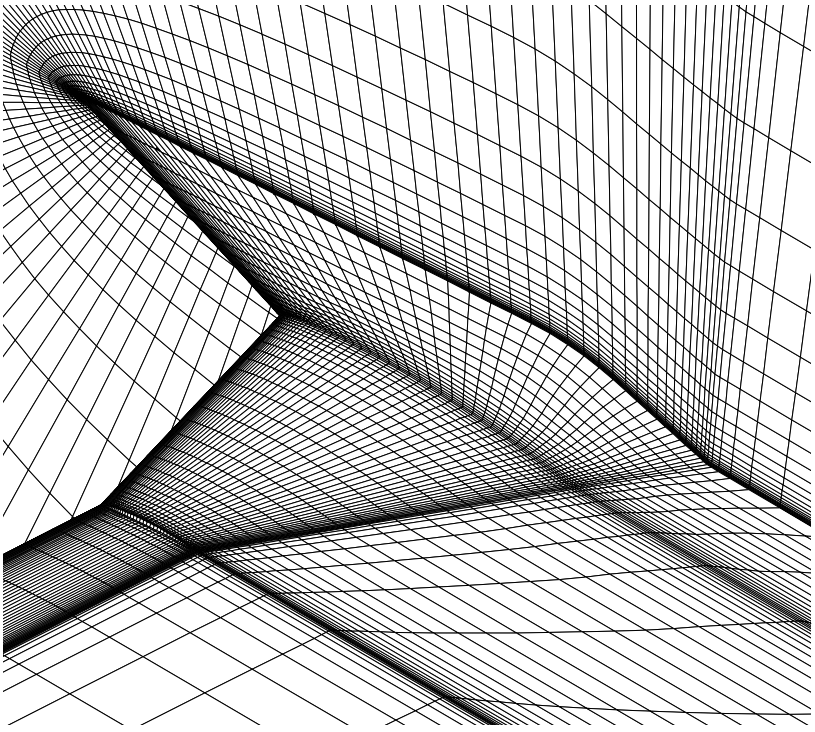

Figure 3. Computational model wing surface, wake and symmetry plane (standard grid).

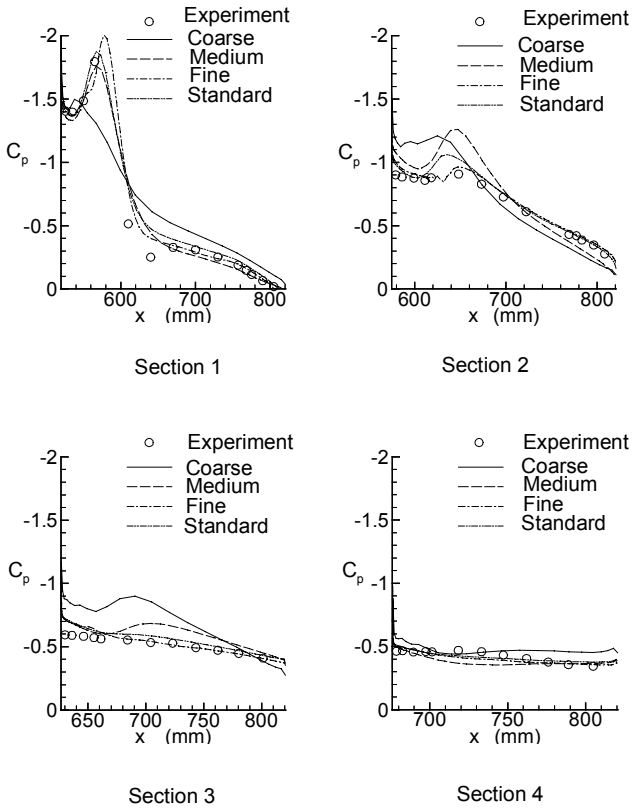

Figure 4. Chordwise pressure coefficient distributions at span sections.
M = 0.601, α = 11.94 degrees, Re = 8 million. Cases 1-4.

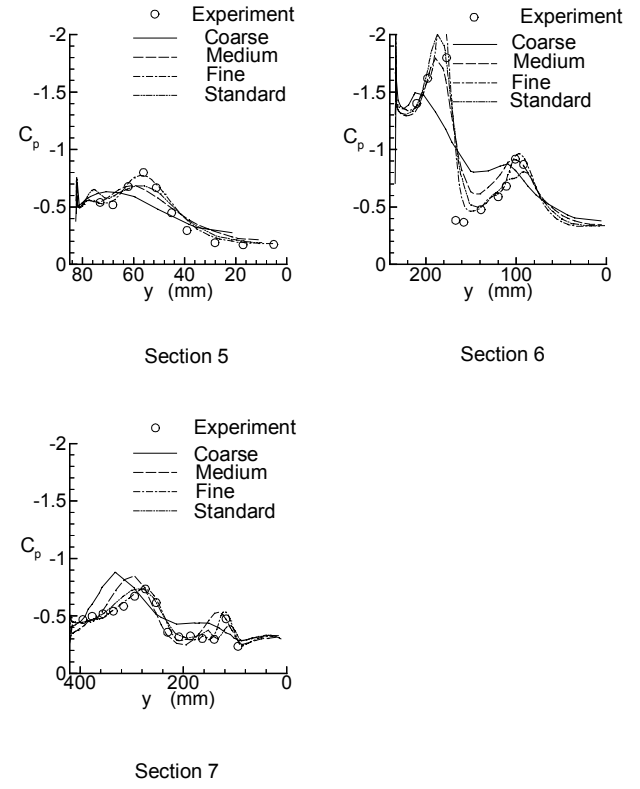

Figure 5. Spanwise pressure coefficient distributions at chord sections.
M = 0.601, α = 11.94 degrees, Re = 8 million. Cases 1-4.

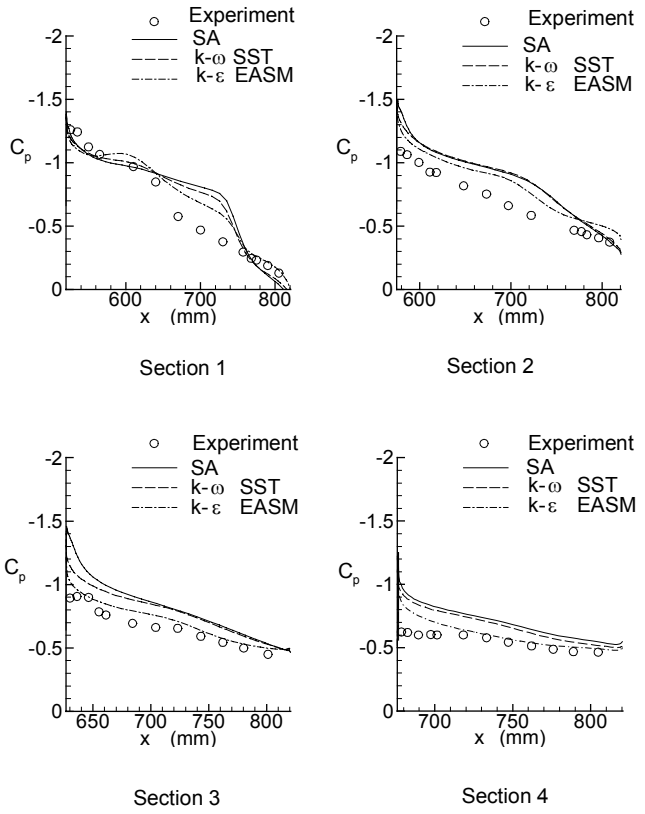

Figure 6. Chordwise pressure coefficient distributions at span sections.
M = 0.899, α = 11.39 degrees, Re = 8 million. Cases 8, 9, 10.

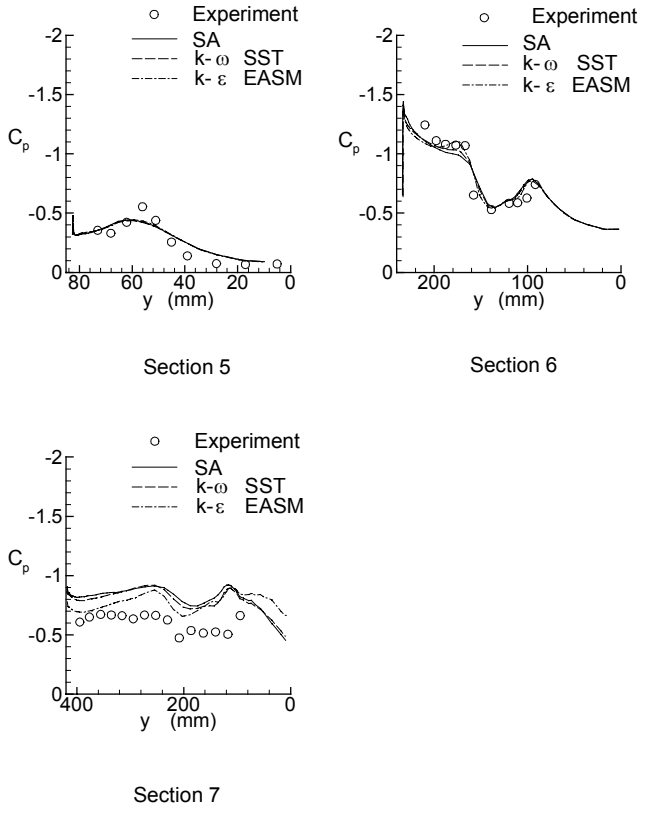

Figure 7. Spanwise pressure coefficient distributions at chord sections.
M = 0.899, α = 11.39 degrees, Re = 8 million. Cases 8, 9, 10.

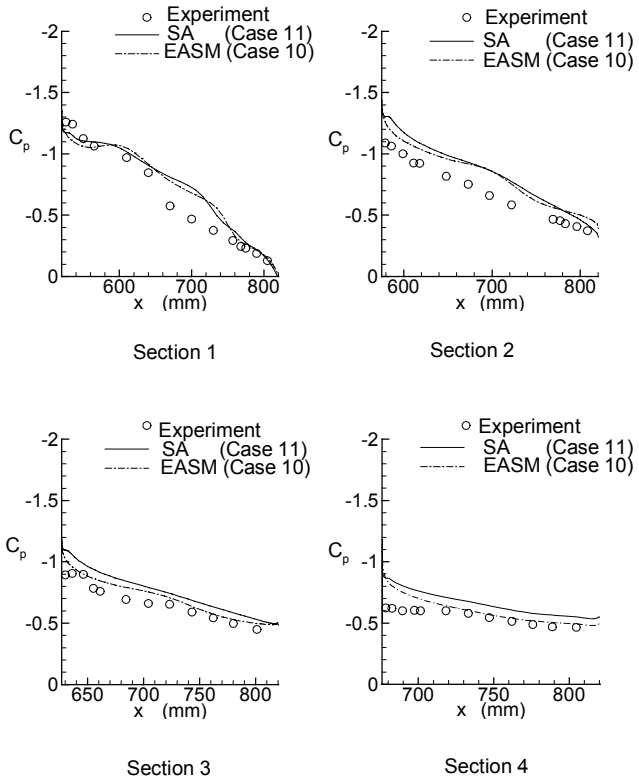

Figure 8. Chordwise pressure coefficient distributions at span sections.
M = 0.899, α = 11.39 degrees, Re = 8 million.

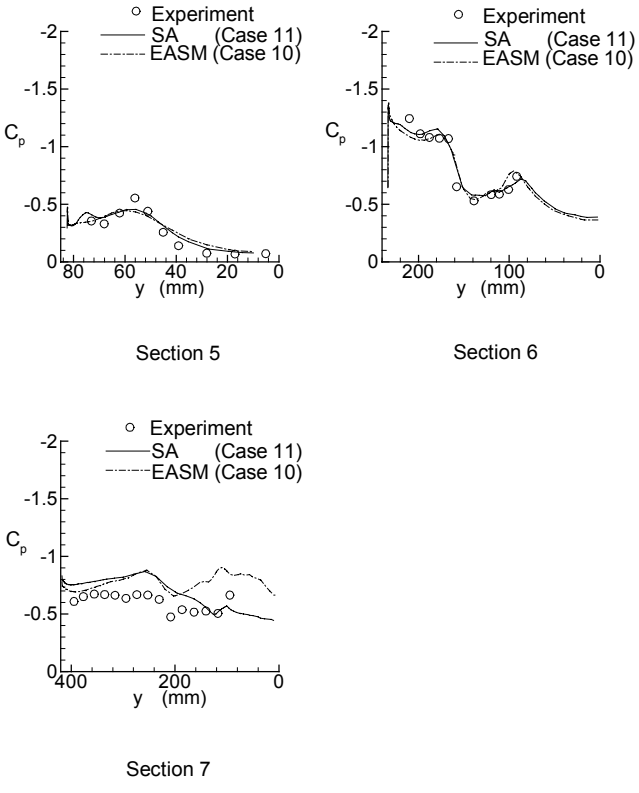

Figure 9. Spanwise pressure coefficient distributions at chord sections.
M = 0.899, α = 11.39 degrees, Re = 8 million.